ISSN 1070-3284, Russian Journal of Coordination Chemistry, 2015, Vol. 41, No. 10, pp. 673–680. © Pleiades Publishing, Ltd., 2015.

Syntheses, Luminescence, and Hirshfeld Surface Analyses of Three Lanthanide Coordination Polymers Directed by Flexible Carboxylate Ligand[1]

L. Lu[a, *], J. Wang[a], A. Q. Ma[b, *], W. P. Wu[a], B. Xie[a], Y. Wu[a], and A. Kumar[c, *]

[a] *School of Chemistry and Pharmaceutical Engineering, Sichuan University of Science and Engineering, Zigong, 643000 P.R. China*

[b] *Guangdong Medical College, School of Pharmacy, Dongguan, 523808 P.R. China*

[c] *Department of Chemistry, Faculty of Science, University of Lucknow, Lucknow, 226007 India*

**e-mail: scwangjun2011@126.com; maqandght@126.com; kumar_abhinav@lkouniv.ac.in*

Received February 22, 2015

Abstract—Three new complexes, namely $\{[Ln(L)_3(2,2'\text{-Bipy})]_n \cdot 2H_2O\}$ (Ln = Pr (**I**), Sm (**II**) and Nd (**III**)) (HL = 3-(4-hydroxyphenyl)propanoic acid), have been synthesized and structurally characterized by single-crystal X-ray diffraction analyses (CIF files CCDC nos. 1045041 (**I**), 1045042 (**II**), 1045043 (**III**)). The structural determination revealed that **I**–**III** have similar dinuclear motifs, which can be further linked into 1D chain via the hydrogen bond interactions. Furthermore, the luminescent properties of **I**–**III** show the strong emissive power and feature.

DOI: 10.1134/S107032841510005X

INTRODUCTION

Coordination polymers of lanthanides have found a variety of applications in materials science including superconductors, luminescent probes and catalysts. Recently it has been demonstrated that luminescent lanthanide compounds have the potential as emitters in electroluminescent devices [1–10]. Although the flexibility of the coordination spheres of the *f*-block metal ions make design difficult, the pliability together with the tendency towards higher coordination numbers makes lanthanide ions attractive for designing different new materials with unusual networks. However, due to the nature of Ln^{3+} ions with partially filled 4*f* orbitals, large radii, and high coordination numbers, they always show characteristic luminescent emissions [11–13]. As a result, studies on luminescent lanthanide compounds are expanding rapidly, and a lot of investigations on the lanthanide frameworks have been published recently [14, 15].

As a building block, 3-(4-hydroxyphenyl)propanoic acid (**HL**) can be multidentate and is an excellent candidate for construction of lanthanide coordination polymers. With the above in mind, we chose HL as ligand to construct MOFs based on the following considerations: (1) HL, as a derivative of the *p*-hydroxybenzoic acid ligand, is a good spacer and has been rarely used in the assembly of coordination polymers; (2) the carboxylic group may have different coordinative mode due to the flexible chain, which may induce higher metal cluster [17]. Up to now, construction of new lanthanide coordination polymers based on HL is not reported, especially involving N-containing ligand. Taking account of the above, we would like to synthesize and explore new complexes with HL and different lanthanide ions. Herein, a series of new Ln coordination polymers based on HL ligand, namely, $\{[Ln(L)_3(2,2'\text{-Bipy})]_n \cdot 2H_2O\}$ (Ln = Pr (**I**), Sm (**II**) and Nd (**III**)), were synthesized under mild conditions and characterized by elemental analyses, IR, TGA, fluorescent measurements, and single-crystal X-ray diffraction analyses. Moreover, compounds **I**–**III** display strong photoluminescent property and high thermal stability.

EXPERIMENTAL

Materials and physical measurements. All the reagents and solvents for synthesis and analysis were commercially available and used directly. Elemental analyses for carbon, hydrogen and nitrogen were performed on a Vario EL III elemental analyzer. The infrared spectra (4000 ~ 600 cm^{-1}) were recorded by using KBr pellet on an AVATAR-370 IR spectrometer. TGA were carried out with a Metter–Toledo TA 50 in dry dinitrogen (60 mL min^{-1}) at a heating rate of 5°C min^{-1}. X-ray power diffraction (**XRPD**) data were recorded on a Rigaku RU200 diffractometer at 60 kV, 300 mA for CuK_α radiation (λ = 1.5406 Å), with a scan speed

[1] The article is published in the original.

Table 1. Crystallographic data and structure refinement details for complexes **I**–**III**

Parameter	Value		
	Pr (**I**)	Nd (**II**)	Sm (**III**)
Formula weight	1655.21	1655.82	1672.09
Crystal system	Triclinic	Triclinic	Triclinic
Space group	$P\bar{1}$	$P\bar{1}$	$P\bar{1}$
a, Å	11.261(6)	11.2368 (9)	11.2382(6)
b, Å	11.925(6)	11.9077(10)	11.8868(9)
c, Å	14.769(7)	14.7521(12)	14.7568(8)
α, deg	88.829(7)	88.619(2)	88.619(5)
β, deg	84.053(8)	83.996(2)	83.873(4)
γ, deg	68.011(7)	68.070(2)	68.270(6)
V, Å^3	1828.7(16)	1828.8(3)	1820.5(2)
Z	1	1	1
ρ_{calcd}, g/cm^3	1.503	1.510	1.525
μ, mm^{-1}	1.394	1.488	1.675
F(000)	842	838	846
θ Range, deg	1.84–25.30	3.16–25.20	2.78–25.40
Reflection collected	9551	30340	13496
Independent reflections, R_{int}	9551 (0.0191)	30340 (0.4401)	13496 (0.0609)
Reflections with $I > 2\sigma$, I	5836	4397	5271
Number of parameters	463	463	458
R_1, wR_2 ($I > 2\sigma(I)$)*	0.0373, 0.1014	0.0786, 0.1226	0.0481, 0.1227
R_1, wR_2 (all data)**	0.0433, 0.1066	0.1849, 0.2156	0.0910, 0.1558

* $R = \Sigma(F_o - F_c)/\Sigma(F_o)$, ** $wR_2 = \{\Sigma[w(F_o^2 - F_c^2)^2]/\Sigma(F_o^2)^2\}^{1/2}$.

of 2°/min and a step size of 0.02° in 2θ. Luminescence spectra for crystal solid samples were recorded at room temperature on an Edinburgh FLS920 phosphorimeter.

X-ray crystallography. Single crystal X-ray diffraction analyses of the compounds were carried out on a Bruker SMART APEX II CCD diffractometer equipped with a graphite monochromated MoK_α radiation (λ = 0.71073 Å) by using ϕ–ω scan technique at room temperature. The intensities were corrected for Lorentz and polarization effects as well as for empirical absorption based on multi-scan techniques; all structures were solved by direct methods and refined by full-matrix least-squares fitting on F^2 by SHELX-97 [18]. Absorption corrections were applied by using multi-scan program SADABS. The hydrogen atoms of organic ligands were placed in calculated positions and refined using a riding on attached atoms with isotropic thermal parameters 1.2 times those of their carrier atoms. In **III**, 38% of the data were observed, which may be attributed to the small measurable crystals and the relatively bad quality of data. The water hydrogen atoms were refined with isotropic thermal parameters 1.5 times those of their carrier atoms. The H atoms of free water molecule were located in a difference Fourier map and then refined as riding in their as-found relative positions with distance restraints of O–H = 0.83 and H–H = 1.38 Å, each within a standard deviation of 0.01 and 0.02 Å, respectively. Table 1 shows crystallographic data of **I**–**III**. Selected bond distances and bond angles are listed in Table 2. Some H-bonded parameters are listed in Table 3.

Supplementary material has been deposited with the Cambridge Crystallographic Data Centre (CCDC nos. 1045041 (**I**), 1045042 (**II**), 1045043 (**III**); deposit@ccdc.cam.ac.uk or http://www.ccdc.cam.ac.uk).

Hirshfeld surface analysis. Molecular Hirshfeld surfaces [19] in the crystal structure were constructed on the basis of the electron distribution calculated as the sum of spherical atom electron densities [20, 21]. For a given crystal structure and a set of spherical atomic densities, the Hirshfeld surface is unique [21]. The normalized contact distance (d_{norm}) based on both d_e and d_i (where d_e is distance from a point on the sur-

Table 2. Selected bond distances (Å) and angles (deg) of structures **I**–**III**

Bond	*d*, Å	Bond	*d*, Å
		I	
Pr(1)–O(1)	2.562(4)	Pr(1)–O(2)	2.631(3)
Pr(1)–O(4)	2.414(4)	Pr(1)–O(7)	2.527(4)
Pr(1)–O(8)	2.610(3)	Pr(1)–N(1)	2.649(5)
Pr(1)–N(2)	2.660(5)		
		II	
Nd(1)–O(1)	2.529(7)	Nd(1)–O(2)	2.613(7)
Nd(1)–O(4)	2.498(8)	Nd(1)–O(5)	2.587(6)
Nd(1)–O(7)	2.404(7)	Nd(1)–N(1)	2.634(8)
Nd(1)–N(2)	2.645(11)		
		III	
Sm(1)–O(1)	2.503(4)	Sm(1)–O(2)	2.610(5)
Sm(1)–O(4)	2.372(5)	Sm(1)–O(7)	2.382(6)
Sm(1)–N(1)	2.607(5)	Sm(1)–N(2)	2.628(5)
Angle	ω,deg	Angle	ω, deg
		I	
O(1)Pr(1)O(2)	49.88(12)	O(1)Pr(1)O(4)	125.89(12)
O(1)Pr(1)O(7)	143.91(13)	O(1)Pr(1)N(2)	69.65(14)
O(1)Pr(1)N(1)	83.67(12)	O(2)Pr(1)O(7)	144.42(10)
O(2)Pr(1)O(8)	138.36(11)	O(4)Pr(1)O(8)	70.32(10)
O(4)Pr(1)O(7)	79.67(11)	O(4)Pr(1)N(2)	137.52(13)
		II	
O(1)Nd(1)O(2)	50.1(2)	O(1)Nd(1)O(4)	144.3(3)
O(1)Nd(1)O(5)	153.6(2)	O(1)Nd(1)O(7)	125.4(2)
O(1)Nd(1)N(1)	84.2(2)	O(1)Nd(1)N(2)	70.3(3)
O(2)Nd(1)O(4)	143.6(2)	O(2)Nd(1)O(5)	137.6(3)
O(2)Nd(1)N(1)	74.9(2)	O(2)Nd(1)N(2)	108.1(2)
		III	
O(1)Sm(1)O(2)	50.79(15)	O(1)Sm(1)O(4)	126.25(15)
O(2)Sm(1)N(2)	108.16(16)	O(4)Sm(1)O(7)	74.71(16)
O(4)Sm(1)N(1)	79.60(17)	O(4)Sm(1)N(2)	137.62(2)
O(7)Sm(1)N(1)	143.28(17)	O(7)Sm(1)N(2)	147.64(16)

face to the nearest nucleus outside the surface and d_i is distance from a point on the surface to the nearest nucleus inside the surface) and the vdW radii of the atom, as given by Eq. (1) enables identification of the regions of particular importance to intermolecular interactions. The combination of d_e and d_i in the form of two-dimensional (2D) fingerprint plot [22, 23] provides a summary of intermolecular contacts in the crystal [19]. The Hirshfeld surfaces mapped with d_{norm} and 2D fingerprint plots were generated using the Crystal-Explorer 2.1 [23]. Graphical plots of the molecular Hirshfeld surfaces mapped with d_{norm} used a red-white-blue colour scheme, where red highlight shorter contacts, white represents the contact around vdW separation, and blue is for longer contact. Additionally, two further coloured plots representing shape index and curvedness based on local curvatures are also presented in this paper [24].

$$d_{norm} = \frac{d_i - r_i^{vdW}}{r_i^{vdW}} + \frac{d_e - r_e^{vdW}}{r_e^{vdW}}.$$

Table 3. Geometric parameters of hydrogen bonds for **I**–**III**

Distance, Å		Angle OHO, deg	
		I	
O(9)···O(1)	2.725(8)	O(9)–H(1)···O(1)	165
O(6)···O(1*w*)	2.695(7)	O(6)–H(2)···O(1*w*)	176
O(3)···O(2)	2.697(5)	O(3)–H(3)···O(2)	171
O(1*w*)···O(3)	2.862(6)	O(1*w*)–H(1*wB*)···O(3)	150
O(1*w*)···O(2*w*)	2.741(9)	O(1*w*)–H(1*wA*)···O(2*w*)	160
O(2*w*)···O(9)	2.840(7)	O(2*w*)–H(2*wA*)···O(9)	139
O(2*w*)···O(6)	3.028(7)	O(2*w*)–H(2*wB*)···O(6)	108
		II	
O(3)···O(2)	2.710(12)	O(3)–H(3)···O(2)	155
O(9)···O(1*w*)	2.691(15)	O(9)–H(9)···O(1*w*)	113
O(6)···O(1)	2.755(14)	O(6)–H(6)···O(1)	166
O(76)···O(7)	3.141(14)	O(76)–H(76)···O(7)	131
		III	
O(2*w*)···O(9)	2.833(9)	O(2*w*)–H(2*wB*)···O(9)	164.00
O(3)···O(2)	2.695(7)	O(3)–H(3)···O(2)	170.00
O(9)···O(1)	2.737(9)	O(9)–H(9)···O(1)	167.00
O(2*w*)···O(6)	3.017(9)	O(2*w*)–H(2*wA*)···O(6)	141.00
O(6)···O(1*w*)	2.688(9)	O(6)–H(6)···O(1*w*)	134.00

Synthesis of complex I. A mixture of H_2O (10 mL) and CH_3OH (5 mL) solution containing HL (0.1 mmol) and was added $Pr(NO_3)_2 \cdot 4H_2O$ (0.15 mmol) in water at 60°C. The pH of the resulting solution was adjusted to 6 using dilute NaOH (0.1 mol/L) and kept at room temperature to prepare compound **I**. From that solution, crystals suitable for X-ray measurements were obtained. The yield was 50%.

For $C_{37}H_{38}N_2O_{11}Pr$ (M = 827.60)

anal. calcd., %:	C, 53.70;	N, 3.38;	H, 4.63.
Found, %:	C, 53.41;	N, 3.25;	H, 4.51.

IR (KBr; ν, cm^{-1}): 3505 v, 3117 m, 1587 v.s, 1519 v, 1445 v.s, 1234 v.s, 1091 m, 880 m, 824 v.s, 743 m, 635 m.

Synthesis of II was carried out by a similar way used for **I**, except that $Pr(NO_3)_2 \cdot 4H_2O$ was replaced by $Sm(NO_3)_2 \cdot 4H_2O$ (0.1 mmol). The yield was 45%.

For $C_{37}H_{38}N_2O_{11}Sm$ (M = 838.05)

anal. calcd., %:	C, 53.09;	N, 3.35;	H, 4.58.
Found, %:	C, 53.11;	N, 3.28;	H, 4.40.

IR (KBr; ν, cm^{-1}): 3501 v, 3115 m, 1589 v.s, 1508 v, 1447 v.s, 1230 v.s, 1095 m, 882 m, 820 v.s, 741 m, 639 m.

Synthesis of III was carried out by a similar way used for **I**, except that $Pr(NO_3)_2 \cdot 4H_2O$ was replaced by $Nd(NO_3)_2 \cdot 4H_2O$ (0.1 mmol). The yield was 40%.

For $C_{37}H_{38}N_2O_{11}Nd$ (M = 830.94)

anal. calcd., %:	C, 53.48;	N, 3.37;	H, 4.61.
Found, %:	C, 53.40;	N, 3.19;	H, 4.46.

IR (KBr; ν, cm^{-1}): 3504 v, 3111 m, 1589 v.s, 1518 v, 1443 v.s, 1233 v.s, 1091 m, 885 m, 829 v.s, 741 m, 634 m.

RESULTS AND DISCUSSION

Compounds **I**–**III** are isostructural and feature dinuclear structures; herein, only the structure of **I** will be discussed in detailed as a representation. The asymmetric unit of **I** contains one Pr^{3+} ion, three L ligands, one 2,2'-Bipy, two lattice water molecules. As shown in Fig. 1, Pr^{3+} ion is nine-coordinated by four oxygen atoms from two η^1-η^1-μ_1 carboxylate groups of L ligands, two oxygen atoms from η^1-η^1-μ_2 carboxy-

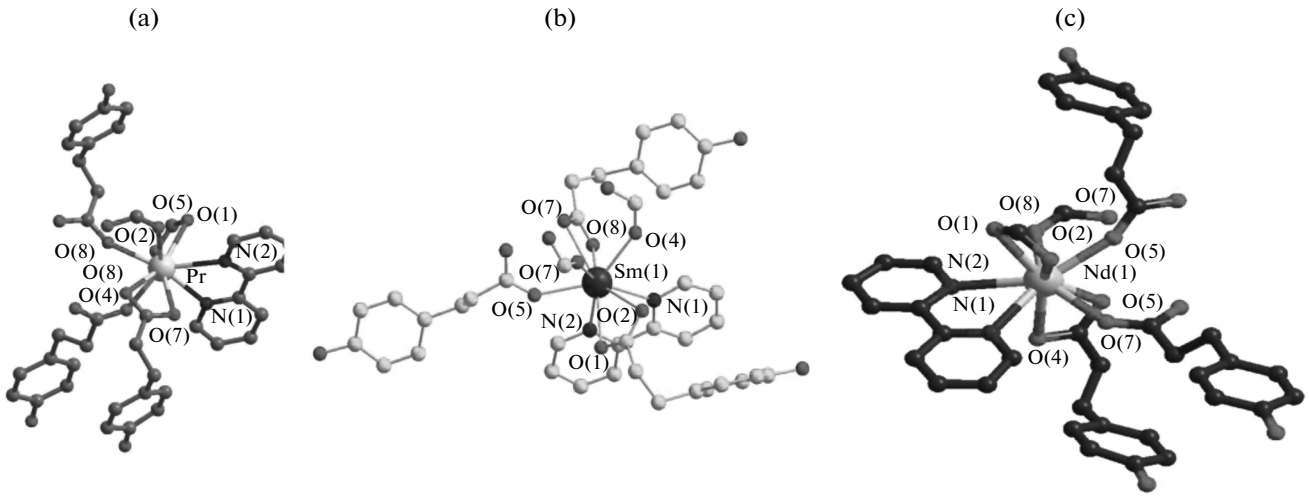

Fig. 1. The coordination geometries of the metal centers and the ligand geometry in **I** (a), **II** (b) and **III** (c). Displacement ellipsoids are drawn at the 30% probability level and H atoms are omitted for clarity.

late groups of L ligands, three oxygen atoms from η^1-η^2-μ_2 carboxylate groups of L ligands, and two nitrogen atoms from 2,2'-Bipy molecules (Fig. 1). The L ligands show three different coordinative modes, resulting in a dinuclear unit with the separations between two neighboring Pr^{3+} ions being 4.01 Å. In addition, careful analysis reveals that the hydrogen bonded interaction association of solvent water molecules, phenolic groups and carboxylate groups in **I** leads to the formation of 1D supramolecular network. The oxygen atom (O(1*w*)) of water molecule could take as donor and acceptor to bind with O(2*w*), and O(6), respectively (Table 3), thus, a dimeric water cluster can be formed. The oxygen atom (O(2*w*)) could take as donor to bind with O(9) from hydroxyl groups. Also, the O(6) from hydroxyl group taking as donor involves in O(4) of carboxylate into a 1D chain, which are cross-lined by other H-bonded interactions between phenolic groups and free water molecules. It should be noted that there is not any packing interaction between rings from adjacent 2,2'-Bipy molecules as shown in Fig. 2.

As to FT–IR spectra, both the compounds show a broad band centered around 3505 cm^{-1} attributable to the O–H stretching frequency of the water cluster in **I**–**III**. The O–H stretching vibration for **I** appears as a broad band centered around 3500 cm^{-1}. Specifically, asymmetric stretching vibration $\nu(COO^-)$ appear around 1596 cm^{-1} for **I**–**III**, and the symmetric stretching vibration $\nu(COO^-)$ are observed 1433 cm^{-1} for **I**–**III** [10]. For the two complexes, the difference between the asymmetric and symmetric stretches, $\Delta\nu_{as}(COO^-) - \nu_s(COO^-)$, are on the order of 160 cm^{-1} indicating that carboxyl groups are coordinated to the metal in a bidentate modes [20], consistent with the observed X-ray crystal structures of **I**–**III**.

To study the stability of the polymers, thermogravimetric analyses (**TGA**) of complexes **I**–**III** were researched. The TGA results of **I**–**III** show the same weight loss steps. Only weight loss character of the compound **I** was discussed. The first weight loss began at 38°C and completed at 95°C. The observed weight loss of 4.2% is corresponding to the loss of coordinated water molecules (calcd. 4.3%). After 195°C, the elimination of organic ligands was observed.

Additionally, to confirm the phase purity and stability of compounds **I**–**III**, the original samples were both characterized by X-ray powder diffraction. Although the experimental patterns have a few unindexed diffractions lines and some are slightly broadened in comparison to those simulated from single-crystal models, it can still to be considered that the bulk synthesized materials and as-grown crystal are homogeneous for compounds **I**–**III**.

Metal-organic hybrid coordination polymers with lanthanide metal centers have been widely investigated for their fluorescence properties [25–27]. The lanthanides only exhibit weak emissions under direct excitation due to their low molar absorption. Lanthanide centered emission can be sensitized by coordinating ligands with π-systems, which can efficiently absorb and transfer the energy. The fluorescence behaviors of **I**–**III** were investigated at room temperature under the same excitation wavelength of 315 nm with the same interval of 3 nm, but only compound **III** shows an intense luminescence property. As shown in Fig. 3, emission peaks of **III** at 625 nm can be obtained under the excitation wavelength, which corresponds to $^5D_0 \rightarrow {}^7F_n$ (n = 1–4) transitions of Nd(III), respectively, indicating a moderately efficient ligand-to-metal energy transfer [28]. The observation of the

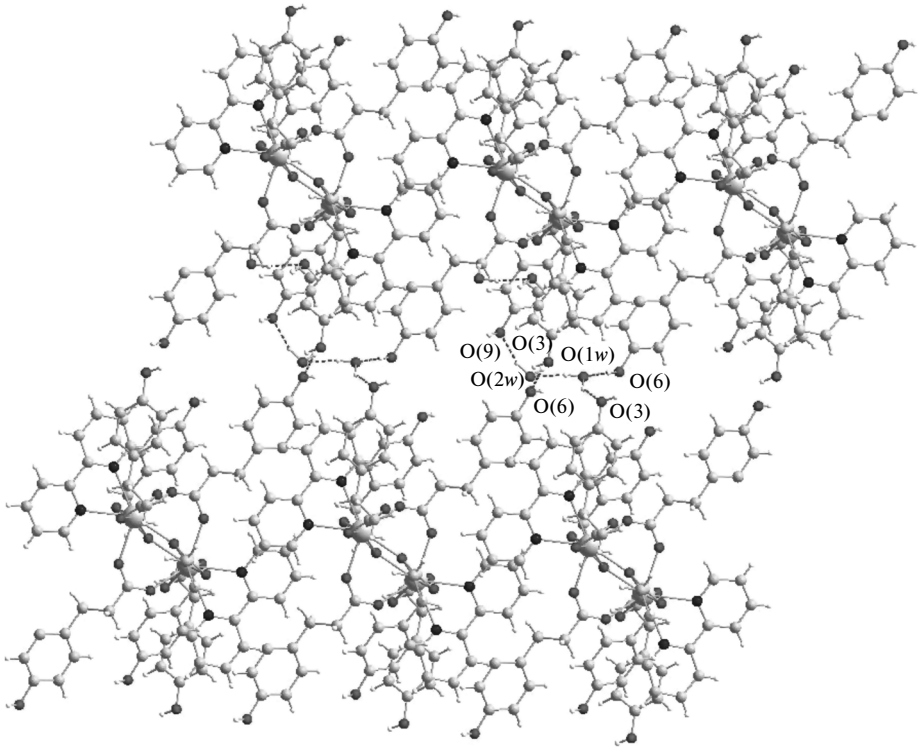

Fig. 2. Viewing of the 2D supramolecular layer along the *xy* plane.

symmetry-forbidden emission $^5D_0 \rightarrow {}^7F_1$ reveals the Nd^{3+} in **III** occupies sites with symmetry and an inversion center. The intensity of the $^5D_0 \rightarrow {}^7F_3$ transition is extremely sensitive to chemical bonds in the vicinity of Nd^{3+}, which increase as the sites symmetry of Nd^{3+} center decrease, while the intensity of the $^5D_0 \rightarrow {}^7F_2$ transition depends only slightly on the nature of the environment of the Nd^{3+} center. The fluorescence emission of HL can be observed at 387 nm. Thus, the emission is due to LMCT [29, 30]. Indeed the emission bands of the ligand molecule do not appear in the spectra; thus, the ligand transfers the excitation energy efficiently to the Nd^{3+} ions.

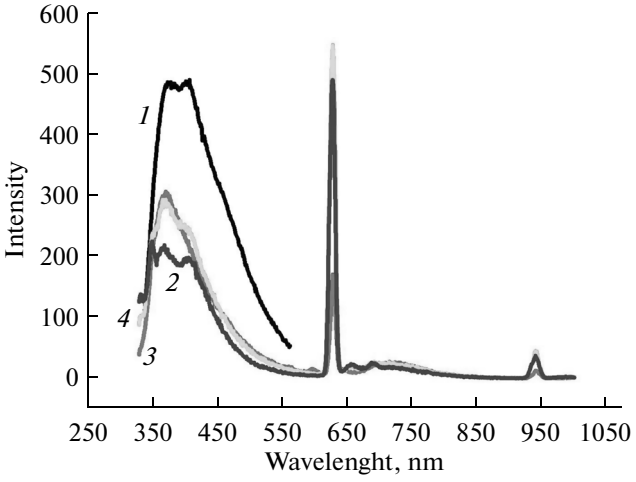

Fig. 3. Emission spectra of compounds HL^1 (*1*), **I** (*2*), **II** (*3*), **III** (*4*) at room temperature.

The Hirshfeld surfaces for the Pr complex is illustrated in Fig. 4 showing surfaces that have been mapped over a d_{norm} range of –0.5 to 1.5 Å, shape index (–1.0 to 1.0 Å) and curvedness (–4.0 to 0.4 Å). The surfaces are shown as transparent to allow visualization of all the atoms of the molecule around which they were calculated. The weak interaction information discussed in X-ray crystallography section is summarized effectively in the spots, with the large circular depressions (deep red) visible on the d_{norm} surfaces indicative of hydrogen bonding contacts. The dominant interactions between O–H···O for the Pr complex can be seen in Hirshfeld surface plots as the bright red shaded area in Fig. 4.

The fingerprint plots for Pr complex are presented in Fig. 5. The O···H intermolecular interactions appear as two distinct spikes of almost equal lengths in the 2D fingerprint plots in the region $2.03 \text{ Å} < (d_e + d_i) < 2.47 \text{ Å}$ as light sky-blue pattern in full fingerprint 2D plots. Complementary regions are visible in the fingerprint plots where one molecule acts as a donor ($d_e > d_i$) and the other as an acceptor ($d_e < d_i$). The fingerprint plots

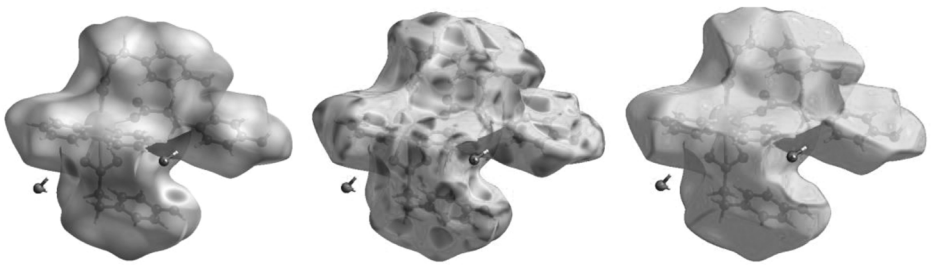

Fig. 4. Hirshfeld surfaces mapped with d_{norm}, shape index and curvedness for the Pr complex.

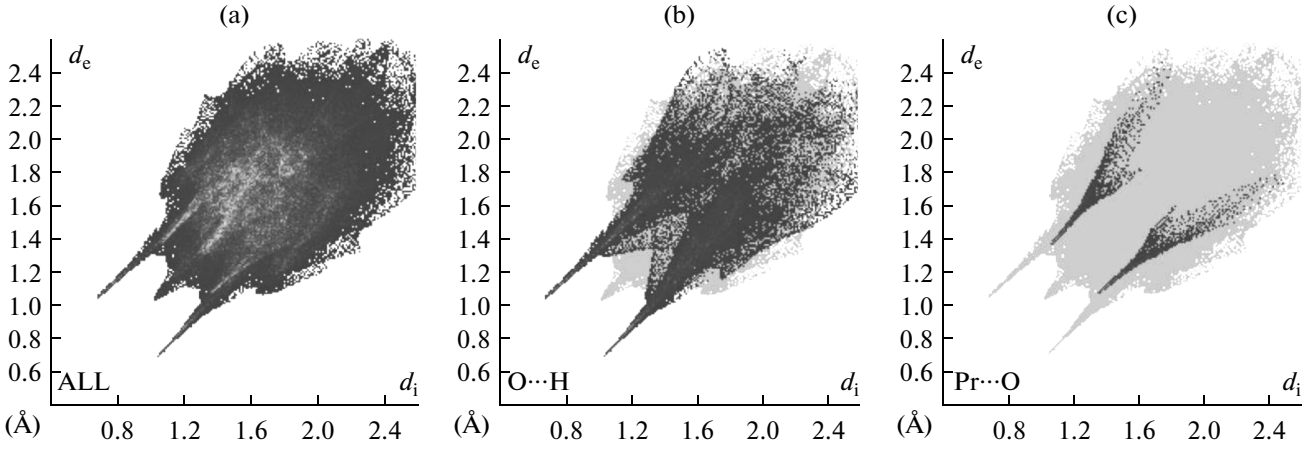

Fig. 5. Fingerprint plots Full (a), resolved into O···H (b) and resolved into Pr···O (c) for compound **I**.

can be decomposed to highlight particular atom pair close contacts. This decomposition enables separation of contributions from different interaction types, which overlap in the full fingerprint. The proportion of O···H for Pr complex is 21.5% of the total Hirshfeld surface. In addition closer look in the fingerprint plot reveals that the complex also exhibits weak Pr···O interactions which constitutes constitutes 2.5% of the total Hirshfeld surface.

ACKNOWLEDGMENTS

The authors acknowledge financial assistance from Sichuan University of Science and Engineering (nos. 2014PY01 and 2015PY03), and the Education Committee of Sichuan Province (no. 12ZA090, 14ZB0220, 15ZB0222, 15ZB0214).

REFERENCE

1. Lippert, B. and Miguel, P.J., *Chem. Soc. Rev.*, 2011, vol. 40, p. 4475.
2. Du, M., Zhang, Z.H., You, Y.P., et al., *CrystEngComm*, 2008, vol. 10, p. 306.
3. Liu, K., Zhu, G.X., Chen, H., et al., *CrystEngComm*, 2008, vol. 10, p. 1527.
4. Chen, B.L., Xiang, S.C., and Qian, G.D., *Acc. Chem. Res.*, 2010, vol. 43, p. 111.
5. Liu, J.Q., Wu, J., Wang, Y.Y., et al., *J. Coord. Chem.*, 2012, vol. 65, p. 1303.
6. Liu, J.Q., Wang, Y.Y., Liu, P., et al., *CrystEngComm*, 2009, vol. 11, p. 207.
7. Liu, J.Q., Wang, Y.Y., Zhang, Y.N., et al., *Eur. J. Inorg. Chem.*, 2009, vol. 2009, p. 147.
8. Liu, J.Q., Wang, Y.Y., and Jia, Z.B., *Inorg. Chem. Commun.*, 2011, vol. 2011, p. 519.
9. Liu, J.Q., Wang, Y.Y., and Huang, Y.S., *CrystEng-Comm.*, 2011, vol. 13, p. 3733.
10. Carlucci, L., Ciani, G., Moret, M., et al., *Angew. Chem. Int. Ed.*, 2000, vol. 39, p. 1506.
11. Ma, S., Yuan, D., Wang, X.S., et al., *Inorg. Chem*, 2009, vol. 48, p. 2072.
12. Sarma, R., Deka, H., Boudalis, A.K., et al., *Cryst. Growth. Des.*, 2011, vol. 11, p. 547.
13. Meng, Q.H., Qiu, T.R., Han, L., et al., *J. Coord. Chem.*, 2010, vol. 63, p. 3165.
14. An, Q., Ren, Y., Chen, S., et al., *J. Coord. Chem.*, 2008, vol. 61, p. 3904.
15. Lin, F.L., Xu, L., Bi, B., et al., *CrystEngComm*, 2008, vol. 10, p. 693.
16. Li, X. and Zhang, Z.Y., *J. Coord. Chem.*, 2007, vol. 59, p. 1873.

17. Seward, C., Hu, N.X., and Wang, S.N., *Dalton Trans.*, 2001, vol. 2001, p. 134.
18. Sheldrick, G.M., *SHELXL-97, Program for Structure Determination and Refinement*, Göttingen (Germany): Univ. of Göttingen, 1997.
19. Spackman, M.A. and McKinnon, J.J., *CrystEngComm*, 2002, vol. 4, p. 378.
20. McKinnon, J.J., Spackman, M.A., and Mitchell, A.S., *Acta. Crystallogr., B*, 2004, vol. 60, p. 627.
21. Rohl, A.L., Moret, M., Kaminsky, W., et al., *Cryst. Growth. Des.*, 2008, vol. 8, p. 4517.
22. Parkin, A., Barr, G., Dong, W., et al., *CrystEngComm*, 2007, vol. 9, p. 648.
23. Wolff, S.K., Greenwood, D.J., McKinnon, J.J., et al., *Crystal Explorer 2.0*, Perth (Australia): Univ. of Western Australia, 2007.
24. Maheshwary, S., Patel, N., Sathyamurthy, N., et al., *J. Phys. Chem., A*, 2001, vol. 105, p. 10525.
25. Bernstein, J., *Chem. Commun.*, 2005, vol. 2005, p. 5007.
26. Fu, Z.Y., Wu, X.T., Dai, J.C., et al., *Eur. J. Inorg. Chem.*, 2002, vol. 2002, p. 2730.
27. Liu, J.Q., Wang, Y.Y., Batten, S.R., et al., *Inorg. Chem. Commun.,* 2012, vol. 19, p. 27.
28. Liu, J.Q., Wang, Y.Y., Wu, T., et al., *CrystEngComm*, 2012, vol. 14, p. 2906.
29. Wang, X.L., Guo, Y.Q., Li, Y.G., et al., *Inorg. Chem.,* 2003, vol. 42, p. 4135.
30. Faulkner, S. and Pope, S.J.A., *J. Am. Chem. Soc.,* 2003, vol. 125, p. 10526.